bioRxiv preprint doi: https://doi.org/10.1101/2022.09.20.508712; this version posted September 20, 2022. The copyright holder for this preprint (which was not certified by peer review) is the author/funder, who has granted bioRxiv a license to display the preprint in perpetuity. It is made available under aCC-BY-NC-ND 4.0 International license.

Title: N6-Adenosine methylation regulates the translation of insulin mRNA

Authors: Daniel Wilinski[1] and Monica Dus[1]*

Affiliations:

[1] Department of Molecular, Cellular, and Developmental Biology, The University of Michigan; Ann Arbor, MI 48109

*Corresponding author. Email: mdus@umich.edu

Abstract:

Relatively little is known about the first step of insulin synthesis: the translation of the mRNA. Here we show that the translation of *D. melanogaster insulin 2* mRNA (*dilp2*) is controlled by methylation of N6-adenosine (m^6A) in the 3' UTR. Mutations in the m^6A writer *Mettl3* and methylated-residues in the *dilp2* 3'UTR decreased the levels of *dilp2* mRNA associated with the polysomes, and the total amount of dilp2 protein produced. This resulted in aberrant energy homeostasis and diabetic-like phenotypes, consistent with the specific function of dilp2 in adult metabolism. Conserved m^6A signatures were also identified in the 3' UTRs of vertebrate insulin mRNAs. These data identify m^6A as a key regulator of insulin protein synthesis and energy homeostasis in metazoans and demonstrate an essential role for m^6A in translation, with important implications for diabetes and metabolic disease.

One-Sentence Summary: The most abundant modification in eukaryotic mRNAs controls the synthesis of insulin protein in *D. melanogaster.*

bioRxiv preprint doi: https://doi.org/10.1101/2022.09.20.508712; this version posted September 20, 2022. The copyright holder for this preprint (which was not certified by peer review) is the author/funder, who has granted bioRxiv a license to display the preprint in perpetuity. It is made available under aCC-BY-NC-ND 4.0 International license.

Main Text:

m^{6}A is an abundant internal modification of eukaryotic mRNAs involved in regulating mRNA stability, turnover, and translation (*1*). As such, it plays an important role in many biological processes, including differentiation, development, and cancer (*2*). Recent studies have also implicated the m^{6}A pathway in energy homeostasis, particularly in the pathogenesis of Type 2 Diabetes (T2D), a chronic disease characterized by the inability to regulate blood glucose via the insulin hormone. Genetic depletion of m^{6}A levels in mammalian insulin β-cells resulted in higher circulating glucose and diabetic phenotypes (*3*, *4*) as well as impaired insulin-cell mass and maturation *in vitro* (*4*). Reduced m^{6}A levels were also observed in the pancreatic β-cells of humans with T2D (*5*). These observations suggest that m^{6}A plays a role in energy homeostasis, especially glucose regulation and T2D. However, the specific mechanisms through which this pathway controls energy balance remain unresolved. Further, translational control is thought to be a critical step in the production of insulin, but the mechanism remains uncharacterized (*6*, *7*). Here we took advantage of the ancestral conservation of the m^{6}A (*8*) and insulin systems in invertebrates (*9*) to identify the molecular mechanisms through which m^{6}A regulates glucose homeostasis and its contributions to diabetes and metabolic disease.

In *D. melanogaster*, 14 neuroendocrine cells located in the *pars intercelebralis* (Fig. 1A) regulate hemolymph glycemia and energy homeostasis by producing three insulin-like hormones (*10*). While these insulin-like hormones have redundant roles in development, the *Drosophila* insulin-like 2 (dilp2) peptide is necessary and sufficient to regulate hemolymph glycemia and fat levels in adult flies; dilp2 also has the highest homology to human insulin, while other dilps are related to the Relaxin family of hormones (*9*, *11*–*13*). Mutations in *dilp2* and ablation of the insulin-producing cells result in higher levels of circulating sugar and reduced metabolic function, phenotypes that can be rescued by injection of human insulin (*9*–*12*). Networks of transcripts involved in fly metabolism are methylated (*14*, *15*). The accessible location of these cells, together with the genetic and metabolic analysis tools available, makes the fly a uniquely suited model to investigate the *in vivo* function of the m^{6}A pathway in glucose and energy homeostasis.

To tackle this question, we first measured the levels of circulating glucose and of body triglycerides in flies mutant for the conserved methyltransferase writer enzyme *Mettl3 (1).* Compared to control flies, *Mettl3*$^{-/-}$ mutants showed higher fasted circulating sugar levels (Fig. 1B), as well as increased triglycerides, as previously reported for *dilp2* mutants (*12*) (Fig. 1C). Cell-specific knockdown of *Mettl3* in the insulin-producing cells using the *Dilp2-GAL4* transgene (50% efficiency, Fig S1A) phenocopied the effects of *Mettl3*$^{-/-}$ mutants and resulted in higher

bioRxiv preprint doi: https://doi.org/10.1101/2022.09.20.508712; this version posted September 20, 2022. The copyright holder for this preprint (which was not certified by peer review) is the author/funder, who has granted bioRxiv a license to display the preprint in perpetuity. It is made available under aCC-BY-NC-ND 4.0 International license.

circulating glucose and triglycerides (Fig. 1D, E). These phenotypes did not arise from developmental alterations in the dilp2+ cells because knocking down *Mettl3* only in post-eclosion, adult *dilp2>Mettl3^{RNAi}; tubulin-GAL80^{ts}* flies showed the same energy homeostasis phenotypes as *dilp2>Mettl3^{RNAi}* animals (Fig. S1B). Importantly, expression of wild-type *Mettl3* only in the insulin cells in an otherwise *Mettl3$^{-/-}$* mutant background rescued the energy balance defects, indicating that the phenotype arises from these cells (Fig. 1F). Thus, *Mettl3* acts in the insulin cells to regulate energy balance; this is similar to the phenotypes of m^{6}A writers mutants observed in mice (*3*).

Since the physiological effects of *Mettl3* depletion are reminiscent of those caused by mutations in the *dilp2* gene –but not other insulin-like peptides (*12*)– and murine data implicated potential changes in insulin levels (*3*, *5*), we asked if *Mettl3* affected the amount of this hormone. We found no changes in the abundance of *dilp2* mRNA between *Mettl3$^{-/-}$* and control flies (Fig. 2A); the amount of other insulin-like mRNAs produced in these cells, *dilp3* and *dilp5*, were unchanged (Fig. S2A, B). In contrast, we observed a marked reduction in dilp2 protein in the insulin-producing cells of *Mettl3$^{-/-}$* mutant flies (Fig. 2B, C); no changes in the number and morphology of the insulin cells, or the amounts of the closely related dilp3 hormone were observed (Fig. S2C, D, E). m^{6}A regulates both RNA stability/turnover and translation in a context-dependent way (*2*). The observed decrease in dilp2 protein levels without accompanying changes in mRNA abundance suggests that m^{6}A may contribute to the translation of the *dilp2* transcript. This may also explain why we do not observe a concomitant transcriptional response from the other dilps (Fig. S2A, B) (*16*). To test the hypothesis that the m^{6}A pathway affects the translational status of the *dilp2* mRNA, we fractionated polysomes from control and *Mettl3$^{-/-}$* mutants and measured the amount of *dilp2* transcript associated with each fraction (Fig. 2D, E). In control flies, 89% of the *dilp2* mRNAs cosedimented with polysome fractions, suggesting active and efficient translation (Fig. 2F, gray). Strikingly, this pattern was reversed in *Mettl3$^{-/-}$* flies, where only 19% of *dilp2* mRNA was found in the heavier fractions; instead, 80% of this mRNA was associated with early fractions, representing ribosomal individual subunits and monosomes (Fig. 2F, green). This suggests that m^{6}A is required for loading the *dilp2* mRNA onto polysomes and therefore proper translation of the *dilp2* mRNA into protein.

To characterize the molecular causes of this phenotype, we used fly heads to perform m^{6}A ultraviolet light-induced Cross-linking and Immunoprecipitation (miCLIP (*17*)), a technique that identifies transcripts marked by m^{6}A. The three biological replicates showed good

bioRxiv preprint doi: https://doi.org/10.1101/2022.09.20.508712; this version posted September 20, 2022. The copyright holder for this preprint (which was not certified by peer review) is the author/funder, who has granted bioRxiv a license to display the preprint in perpetuity. It is made available under aCC-BY-NC-ND 4.0 International license.

reproducibility with a mean correlation of 0.95 (Fig. S3A) and identified 4,506 m^{6}A peaks corresponding to 1,828 genes involved in brain processes including development and plasticity (Data S1 and Fig. S3B). Forty-four percent (2009) of our peaks overlap with previous CLIP data from fly heads including *Atpα* (*18*) (Fig. S3C). Metagene analysis revealed that most m^{6}A peaks mark the 5' untranslated region (UTR) of transcripts, while a much smaller portion is present in the 3' UTR, particularly near the stop codon (Fig. 3A); this is consistent with previous miCLIP studies in flies (*18*, *19*). We also observed an enriched fly RRAC (R=purine) sequence motif at C-to-T crosslinking-induced mutation sites (CIMS) which represent m^{6}A sites from CLIP/RIP data (*14*, *17*–*19*) (Fig. 3B, Data S1).

Since we observed lower translation of the *dilp2* mRNA in *Mettl3*$^{-/-}$ mutants, we asked if this transcript was methylated. Indeed, an m^{6}A peak was present in the 3' UTR of *dilp2*, shortly after the stop codon (Fig. 3C); none of the mRNAs encoding for other insulin-like peptides expressed in the insulin-producing cells, such as *dilp3* or *dilp5*, showed any signatures of methylation (Fig S3D, E). Thus, the *dilp2* mRNA is methylated *in vivo*. To better characterize the location of the modified A we turned to direct-RNA sequencing (Oxford Nanopore) where modified bases can be detected as changes in normalized current through the nanopore (*20*–*22*). We first *in vitro* transcribed RNA oligomers containing only one methylated or unmethylated A, sequenced them on the Nanopore, and then used the EpiNano algorithm to assess deviations in base-calling between these two identical oligomers (Fig. S4A, Table S1) (*21*). Direct-RNA sequencing of these RNAs revealed a shift in the raw current near the methylated bases (Fig. S4B) which results in a significant difference in base-call "errors" (Fig. S4C). Thus, we can detect N6-methylation as a deviation in base calling at or near to the methylated A via direct-RNA sequencing. To define if the native *dilp2* mRNA was methylated *in vivo*, we enriched for insulin-cell-specific mRNAs by expressing the FLAG-tagged Ribosomal Protein 3 *UAS-RPL3::FLAG* transgene with *Dilp2-GAL4*. We then direct-RNA sequenced the purified poly(A)+ RNA and defined deviations between base calls of *in vitro* transcribed and native RNA (*21*). This experiment revealed a significant difference in the 3' UTR between the *in vitro* transcribed and native *dilp2* RNAs (Fig. 3D, E). In particular, three bases in the 3'UTR (Positions G519, C614, C664) had significantly higher base-call deviations in the native RNA compared to the *in vitro* transcribed *dilp2* RNA. Position G519 corresponds to the CLIP peak and positions C614 and C664 are part of AC dinucleotides (Table S2). Together with the results from miCLIP, these data show that at least three specific ACs in the 3'UTR of the *dilp2* mRNA are methylated *in vivo* in the *D. melanogaster* insulin-producing cells.

bioRxiv preprint doi: https://doi.org/10.1101/2022.09.20.508712; this version posted September 20, 2022. The copyright holder for this preprint (which was not certified by peer review) is the author/funder, who has granted bioRxiv a license to display the preprint in perpetuity. It is made available under aCC-BY-NC-ND 4.0 International license.

To investigate whether N-6 RNA methylation of the *dilp2* 3' UTR directly affects its translation, we generated flies that lacked "methylateable" A's in the 3' UTR (*dilp2* $^{m6A-/-}$). Using the miCLIP and Nanopore analyses, we selected 11 "AC" nucleotides and mutated these into "UC" using CRISPR (Fig. S5A). These included the AC near G519 and C614 with the strongest methylation signals (Fig. 3C, E); A663 could not be removed for technical reasons. Clone 364-4 was selected for further study after confirming all the A>U mutations by Sanger sequencing (Fig. S5B). Sucrose density polysome gradients showed that compared to control flies, where 92% of the *dilp2* mRNAs were in heavier fractions, representing the polysomes, 69% of *dilp2* mRNAs from *dilp2* $^{m6A-/-}$ flies were associated with early fractions (Fig 4A, S6A, B). Consistent with this, quantification of the total levels of dilp2 protein with anti-dilp2 specific antibodies in the insulin cells revealed a 20 % decrease in *dilp2* $^{m6A-/-}$ flies compared to controls (Fig. 4B, C). Strikingly, we found that *dilp2* $^{m6A-/-}$ mutants recapitulated the deficits in glucose and energy homeostasis observed in *Mettl3* mutant flies, with an increase in fasting glucose levels and in triglycerides (Fig 4 D, E). Together, these findings suggest that, in flies, m^{6}A modification of the *dilp2* mRNA controls the effective translation, and thus synthesis, of the insulin protein.

Elements in the 3' UTR of mammalian insulin are thought to play an important role in its translation (*6*, *7*). Given the conservation of the insulin and m^{6}A pathways in metazoa, we asked if signatures of m^{6}A were also present in vertebrate insulin mRNAs. To do this, we obtained polyA-selected mRNAs from Atlantic salmon pancreatic tissue (*Salmo salar*) and mouse islet cells and analyzed them by direct-RNA sequencing. We analyzed 5,000 and 10,000 reads that mapped to the INS and INS2 insulin genes from salmon and mouse, respectively. This analysis revealed one putative m^{6}A site in the 3'UTR of salmon insulin (Fig. 4F, Table S2, C464) and two putative m^{6}A sites in INS2 3' UTR (Fig. 4G, Table S2, A531, and C581). This suggests that regulation of insulin translation by m^{6}A may be conserved.

Taken together, our observations support a general model where methylation of adenosines in the 3'UTR of the *dilp2* mRNA enhances translation by promoting the association of this mRNA with polysomes which is consistent with a possible defect in translation initiation (*23*). In contrast, m^{6}A in the 5' UTR has been linked to non-canonical translational control (*24*). Although we cannot exclude that this mechanism also controls other aspects of *dilp2* mRNA, our polysome profiling data links m^{6}A marks in the *dilp2* mRNA with translational initiation. In the absence of this epitranscriptomic signal, less insulin is produced, compromising the animal's ability to regulate sugar and energy homeostasis. Interestingly, this mark only controls the translation of the *dilp2* mRNA and not the closely related *dilp3* and *dilp5* genes, consistent with

bioRxiv preprint doi: https://doi.org/10.1101/2022.09.20.508712; this version posted September 20, 2022. The copyright holder for this preprint (which was not certified by peer review) is the author/funder, who has granted bioRxiv a license to display the preprint in perpetuity. It is made available under aCC-BY-NC-ND 4.0 International license.

the fact that the deposition of the signal is specific (*25*). Further, it suggests that previously observed transcriptional compensations among different insulin-like peptides in *D. melanogaster* are tied to mRNA abundance, not protein levels (*16*).

Based on our discovery that adenosines in the 3'UTR of mouse and salmon insulin mRNAs are marked with m^6A, and on previous data showing that Mettl3 and Mettl14 are involved in glucose homeostasis, we anticipate that regulation of insulin translation and energy homeostasis by this RNA modification will be a conserved mechanism in vertebrates. Since m^6A has been linked to cellular metabolism and signaling, this mode of regulation could provide a mechanism to time insulin translation with the presence of specific physiological signals, as well as to prepare for its fast production. This is consistent with findings that elements in the 3'UTR of mammalian insulin are important for its regulated production (*6*, *7*) and that altered levels of m^6A are found in the islets of people with T2D (*5*). However, it is still unclear if the m^6A mark is dynamic and could really be used to switch translation. However, rather than toggling translation on and off, m^6A could promote protein synthesis by direct cellular compartmentalization via phase separation (*1*). This work also provides direct evidence for the hypothesis that m^6A in the 3' UTR plays an essential and robust role in translation, although the mechanisms remain to be defined (*1*). Besides its relevance to the study of insulin and physiology, the methylation of *dilp2* mRNA could be a viable model to address these and future questions about the biology of m^6A. In summary, our work has uncovered a new fundamental step in the biosynthesis of insulin and the biology of m^6A, with critical implications for understanding RNA control (or translational control) mechanisms in the regulation of energy homeostasis and the etiology of metabolic disease.

References and Notes:

1. S. Zaccara, R. J. Ries, S. R. Jaffrey, Reading, writing and erasing mRNA methylation. *Nat. Rev. Mol. Cell Biol.* **20**, 608–624 (2019).

2. P. C. He, C. He, m6 A RNA methylation: from mechanisms to therapeutic potential. *EMBO J.* **40**, e105977 (2021).

3. L. Men, J. Sun, G. Luo, D. Ren, Acute Deletion of METTL14 in β-Cells of Adult Mice Results in Glucose Intolerance. *Endocrinology*. **160**, 2388–2394 (2019).

4. J. Liu, G. Luo, J. Sun, L. Men, H. Ye, C. He, D. Ren, METTL14 is essential for β-cell survival and insulin secretion. *Biochim. Biophys. Acta Mol. Basis Dis.* **1865**, 2138–2148 (2019).

5. D. F. De Jesus, Z. Zhang, S. Kahraman, N. K. Brown, M. Chen, J. Hu, M. K. Gupta, C. He, R. N. Kulkarni, m6A mRNA Methylation Regulates Human β-Cell Biology in Physiological

bioRxiv preprint doi: https://doi.org/10.1101/2022.09.20.508712; this version posted September 20, 2022. The copyright holder for this preprint (which was not certified by peer review) is the author/funder, who has granted bioRxiv a license to display the preprint in perpetuity. It is made available under aCC-BY-NC-ND 4.0 International license.

States and in Type 2 Diabetes. *Nat Metab*. **1**, 765–774 (2019).

6. H. Jahr, D. Schröder, B. Ziegler, M. Ziegler, H. Zühlke, Transcriptional and translational control of glucose-stimulated (pro)insulin biosynthesis. *Eur. J. Biochem.* **110**, 499–505 (1980).

7. M. G. Magro, M. Solimena, Regulation of β-cell function by RNA-binding proteins. *Molecular Metabolism*. **2**, 348–355 (2013).

8. T. Lence, M. Soller, J.-Y. Roignant, A fly view on the roles and mechanisms of the m6A mRNA modification and its players. *RNA Biol.* **14**, 1232–1240 (2017).

9. R. Das, L. L. Dobens, Conservation of gene and tissue networks regulating insulin signalling in flies and vertebrates. *Biochem. Soc. Trans.* **43**, 1057–1062 (2015).

10. E. J. Rulifson, S. K. Kim, R. Nusse, Ablation of insulin-producing neurons in flies: growth and diabetic phenotypes. *Science*. **296**, 1118–1120 (2002).

11. K. Kannan, Y.-W. C. Fridell, Functional implications of Drosophila insulin-like peptides in metabolism, aging, and dietary restriction. *Front. Physiol.* **4**, 288 (2013).

12. U. V. Semaniuk, D. V. Gospodaryov, K. M. Feden'ko, I. S. Yurkevych, A. M. Vaiserman, K. B. Storey, S. J. Simpson, O. Lushchak, Insulin-Like Peptides Regulate Feeding Preference and Metabolism in Drosophila. *Front. Physiol.* **9**, 1083 (2018).

13. W. Brogiolo, H. Stocker, T. Ikeya, F. Rintelen, R. Fernandez, E. Hafen, An evolutionarily conserved function of the Drosophila insulin receptor and insulin-like peptides in growth control. *Curr. Biol.* **11**, 213–221 (2001).

14. T. Lence, J. Akhtar, M. Bayer, K. Schmid, L. Spindler, C. H. Ho, N. Kreim, M. A. Andrade-Navarro, B. Poeck, M. Helm, J.-Y. Roignant, m6A modulates neuronal functions and sex determination in Drosophila. *Nature*. **540**, 242–247 (2016).

15. I. U. Haussmann, Z. Bodi, E. Sanchez-Moran, N. P. Mongan, N. Archer, R. G. Fray, M. Soller, m6A potentiates Sxl alternative pre-mRNA splicing for robust Drosophila sex determination. *Nature*. **540**, 301–304 (2016).

16. S. Broughton, N. Alic, C. Slack, T. Bass, T. Ikeya, G. Vinti, A. M. Tommasi, Y. Driege, E. Hafen, L. Partridge, Reduction of DILP2 in Drosophila triages a metabolic phenotype from lifespan revealing redundancy and compensation among DILPs. *PLoS One*. **3**, e3721 (2008).

17. A. V. Grozhik, B. Linder, A. O. Olarerin-George, S. R. Jaffrey, Mapping m6A at Individual-Nucleotide Resolution Using Crosslinking and Immunoprecipitation (miCLIP). *Methods Mol. Biol.* **1562**, 55–78 (2017).

18. L. Kan, S. Ott, B. Joseph, E. S. Park, W. Dai, R. E. Kleiner, A. Claridge-Chang, E. C. Lai, A neural m6A/Ythdf pathway is required for learning and memory in Drosophila. *Nat. Commun.* **12**, 1458 (2021).

19. L. Kan, A. V. Grozhik, J. Vedanayagam, D. P. Patil, N. Pang, K.-S. Lim, Y.-C. Huang, B. Joseph, C.-J. Lin, V. Despic, J. Guo, D. Yan, S. Kondo, W.-M. Deng, P. C. Dedon, S. R. Jaffrey, E. C. Lai, The m6A pathway facilitates sex determination in Drosophila. *Nat.*

bioRxiv preprint doi: https://doi.org/10.1101/2022.09.20.508712; this version posted September 20, 2022. The copyright holder for this preprint (which was not certified by peer review) is the author/funder, who has granted bioRxiv a license to display the preprint in perpetuity. It is made available under aCC-BY-NC-ND 4.0 International license.

Commun. **8**, 15737 (2017).

20. D. R. Garalde, E. A. Snell, D. Jachimowicz, B. Sipos, J. H. Lloyd, M. Bruce, N. Pantic, T. Admassu, P. James, A. Warland, M. Jordan, J. Ciccone, S. Serra, J. Keenan, S. Martin, L. McNeill, E. J. Wallace, L. Jayasinghe, C. Wright, J. Blasco, S. Young, D. Brocklebank, S. Juul, J. Clarke, A. J. Heron, D. J. Turner, Highly parallel direct RNA sequencing on an array of nanopores. *Nat. Methods*. **15**, 201–206 (2018).

21. H. Liu, O. Begik, M. C. Lucas, J. M. Ramirez, C. E. Mason, D. Wiener, S. Schwartz, J. S. Mattick, M. A. Smith, E. M. Novoa, Accurate detection of m6A RNA modifications in native RNA sequences. *Nat. Commun.* **10**, 4079 (2019).

22. M. T. Parker, K. Knop, A. V. Sherwood, N. J. Schurch, K. Mackinnon, P. D. Gould, A. J. Hall, G. J. Barton, G. G. Simpson, Nanopore direct RNA sequencing maps the complexity of Arabidopsis mRNA processing and m6A modification. *Elife*. **9** (2020), doi:10.7554/eLife.49658.

23. X. Wang, B. S. Zhao, I. A. Roundtree, Z. Lu, D. Han, H. Ma, X. Weng, K. Chen, H. Shi, C. He, N(6)-methyladenosine Modulates Messenger RNA Translation Efficiency. *Cell*. **161**, 1388–1399 (2015).

24. K. D. Meyer, D. P. Patil, J. Zhou, A. Zinoviev, M. A. Skabkin, O. Elemento, T. V. Pestova, S.-B. Qian, S. R. Jaffrey, 5’ UTR m(6)A Promotes Cap-Independent Translation. *Cell*. **163**, 999–1010 (2015).

25. K. D. Meyer, m6A-mediated translation regulation. *Biochim. Biophys. Acta Gene Regul. Mech.* **1862**, 301–309 (2019).

26. B. J. Zarnegar, R. A. Flynn, Y. Shen, B. T. Do, H. Y. Chang, P. A. Khavari, irCLIP platform for efficient characterization of protein-RNA interactions. *Nat. Methods*. **13**, 489–492 (2016).

27. A. Dobin, C. A. Davis, F. Schlesinger, J. Drenkow, C. Zaleski, S. Jha, P. Batut, M. Chaisson, T. R. Gingeras, STAR: ultrafast universal RNA-seq aligner. *Bioinformatics*. **29**, 15–21 (2013).

28. P. J. Uren, E. Bahrami-Samani, S. C. Burns, M. Qiao, F. V. Karginov, E. Hodges, G. J. Hannon, J. R. Sanford, L. O. F. Penalva, A. D. Smith, Site identification in high-throughput RNA-protein interaction data. *Bioinformatics*. **28**, 3013–3020 (2012).

29. A. O. Olarerin-George, S. R. Jaffrey, MetaPlotR: a Perl/R pipeline for plotting metagenes of nucleotide modifications and other transcriptomic sites. *Bioinformatics*. **33**, 1563–1564 (2017).

30. G. E. Crooks, G. Hon, J.-M. Chandonia, S. E. Brenner, WebLogo: a sequence logo generator. *Genome Res.* **14**, 1188–1190 (2004).

31. G. Yu, L.-G. Wang, Y. Han, Q.-Y. He, clusterProfiler: an R package for comparing biological themes among gene clusters. *OMICS*. **16**, 284–287 (2012).

32. M. Carlson, *org.Dm.eg.db* (Bioconductor, 2017; https://bioconductor.org/packages/org.Dm.eg.db).

bioRxiv preprint doi: https://doi.org/10.1101/2022.09.20.508712; this version posted September 20, 2022. The copyright holder for this preprint (which was not certified by peer review) is the author/funder, who has granted bioRxiv a license to display the preprint in perpetuity. It is made available under aCC-BY-NC-ND 4.0 International license.

33. P. Essers, L. S. Tain, T. Nespital, J. Goncalves, J. Froehlich, L. Partridge, Reduced insulin/insulin-like growth factor signaling decreases translation in Drosophila and mice. *Sci. Rep.* **6**, 30290 (2016).

34. D. Wilinski, J. Winzeler, W. Duren, J. L. Persons, K. J. Holme, J. Mosquera, M. Khabiri, J. M. Kinchen, P. L. Freddolino, A. Karnovsky, M. Dus, Rapid metabolic shifts occur during the transition between hunger and satiety in Drosophila melanogaster. *Nat. Commun.* **10**, 4052 (2019).

35. C. E. May, A. Vaziri, Y. Q. Lin, O. Grushko, M. Khabiri, Q.-P. Wang, K. J. Holme, S. D. Pletcher, P. L. Freddolino, G. G. Neely, M. Dus, High Dietary Sugar Reshapes Sweet Taste to Promote Feeding Behavior in Drosophila melanogaster. *Cell Rep.* **27**, 1675–1685.e7 (2019).

36. C. Géminard, E. J. Rulifson, P. Léopold, Remote control of insulin secretion by fat cells in Drosophila. *Cell Metab.* **10**, 199–207 (2009).

37. K. Buhler, J. Clements, M. Winant, L. Bolckmans, V. Vulsteke, P. Callaerts, Growth control through regulation of insulin signalling by nutrition-activated steroid hormone in Drosophila. *Development*. **145** (2018), doi:10.1242/dev.165654.

38. J. Schindelin, I. Arganda-Carreras, E. Frise, V. Kaynig, M. Longair, T. Pietzsch, S. Preibisch, C. Rueden, S. Saalfeld, B. Schmid, J.-Y. Tinevez, D. J. White, V. Hartenstein, K. Eliceiri, P. Tomancak, A. Cardona, Fiji: an open-source platform for biological-image analysis. *Nat. Methods*. **9**, 676–682 (2012).

39. H. Li, Minimap2: pairwise alignment for nucleotide sequences. *Bioinformatics*. **34**, 3094–3100 (2018).

40. M. Stoiber, J. Quick, R. Egan, J. E. Lee, S. Celniker, R. K. Neely, N. Loman, L. A. Pennacchio, J. Brown, De novoIdentification of DNA Modifications Enabled by Genome-Guided Nanopore Signal Processing, , doi:10.1101/094672.

41. J. M. Tennessen, W. E. Barry, J. Cox, C. S. Thummel, Methods for studying metabolism in Drosophila. *Methods*. **68**, 105–115 (2014).

Acknowledgments:

General: We thank Pierre Léopold for the kind gift of Dilp2 antibody, Patrick Callaerts for the gift of Dilp3 antibody, Randy Seeley for mice and Corentin Cras-Méneur for isolating Mouse islets, Jean-Yves Roignant for *Mettl3* mutant flies, and the Blooming Drosophila Stock center for other flies used in this study. Salmon tissue was a gift from Brian Peterson (USDA); we thank Cunmin Duan for advice. We are grateful to Peter Todd and Shannon Miller for training and for the use of their polysome fractionation equipment and training; Christopher Lapointe for thoughtful comments on the manuscript. We also thank Julia Kuhl for designing some of the graphics in this manuscript.

bioRxiv preprint doi: https://doi.org/10.1101/2022.09.20.508712; this version posted September 20, 2022. The copyright holder for this preprint (which was not certified by peer review) is the author/funder, who has granted bioRxiv a license to display the preprint in perpetuity. It is made available under aCC-BY-NC-ND 4.0 International license.

Funding:

NIH R00 DK-97141 (MD)

NIH 1DP2DK-113750 (MD)

Rita Allen Foundation (MD)

NSF CAREER 1941822 (MD)

NIH T32 DA007268 (DW)

NIH P30 DK089503 (MD and DW)

Author contributions:

Conceptualization: DW and MD

Methodology: DW

Investigation: DW and MD

Visualization: DW and MD

Funding acquisition: MD

Project administration: MD

Supervision: MD

Writing – DW and MD

Writing – review & editing: DW and MD

Competing interests: Authors declare that they have no competing interests.

Data and materials availability: All data are available in the main text or supplementary materials. RNA-sequencing reads were deposited in Gene Expression Omnibus accession number GSE207547. (The following secure token has been created to allow review of record GSE207547 while it remains in private status: cfkreeumnfajzkn) *dllp2* 3'UTR mutants are available upon request.

bioRxiv preprint doi: https://doi.org/10.1101/2022.09.20.508712; this version posted September 20, 2022. The copyright holder for this preprint (which was not certified by peer review) is the author/funder, who has granted bioRxiv a license to display the preprint in perpetuity. It is made available under aCC-BY-NC-ND 4.0 International license.

Supplementary Materials

Materials and Methods

Fly lines and husbandry

All flies were maintained at 25 °C in a humidity-controlled incubator with a 12:12 hr light/dark cycle. Animals were fed Bloomington Food B (cornmeal-glucose) ad-lib and provided fresh food every other day. For all experiments, flies were collected under CO_2 anesthesia, 2–4 days following eclosion, and housed in groups of 20–30 to age until testing (6-10 days old). The stocks used are listed in Table S3. Depending on the genetic background of the mutations, we used w^{1118} (Rainbow Transgenic Flies, Camarillo, CA) or w^{1118} *Canton-S* flies (Benzer lab, Caltech) as controls.

RNA extraction

Standard methods to isolate total RNA were used for quantitative polymerase chain reaction (qPCR), crosslinking and immunoprecipitation (CLIP), and direct-RNA sequencing. Briefly, heads from 10 to 20 flies were dissected and immediately frozen on dry ice for qPCR. 800 fly heads were isolated from bodies by sieving for CLIP and direct RNA-sequencing. All samples were stored at -80 °C until extraction. Phenol-chloroform (Invitrogen, 15596018) and RIPA buffer (150 mm NaCl, 1% Nonidet P-40, 0.5% Sodium deoxycholate, 0.1% SDS, 50mM Tris pH 7.5) were added to frozen samples and homogenized by bead bashing (Bead Ruptor, 19-040E). Phenol-chloroform extracted RNA was precipitated by isopropanol with GlycoBlue coprecipitant (Invitrogen AM9515). RNA was stored at −80 °C until further processing.

CLIP

Library preparation

We adapted miCLIP (*17*) to use infrared-dye-conjugated irCLIP adaptors (*26*). Briefly, 20 ug of poly(A) selected (Invitrogen, 61012) RNA for each biological replicate from 800 heads of w^{1118}*CS* flies was used as input to the CLIP, no antibody control, and input only (no CLIP) reactions. Fragmented RNA (Ambion, E6150S) was incubated for 2 hr at 4 °C with antibody against m^6A (Abcam, ab151230), UV-crosslinked, then immunoprecipitated with magnetic beads (Invitrogen, 10004D) as in (*17*). Pre-adenylated dye-conjugated linkers were ligated (NEB, M0351S) to dephosphorylated 3’ ends of RNA fragments overnight at 16 °C (Table S1).

bioRxiv preprint doi: https://doi.org/10.1101/2022.09.20.508712; this version posted September 20, 2022. The copyright holder for this preprint (which was not certified by peer review) is the author/funder, who has granted bioRxiv a license to display the preprint in perpetuity. It is made available under aCC-BY-NC-ND 4.0 International license.

RNA was extracted with NuPAGE SDS buffer and separated by NuPAGE gel (Invitrogen, NP0321), transferred to nitrocellulose membrane and visualized for excision at 800 nm. RNA-antibody complexes were released from the membrane by proteinase K digestion and RNA was purified with phenol-chloroform extraction. RNA was reverse transcribed (Invitrogen, 18080085), circularized (Lucigen, CL4111K), and PCR-amplified (Thermo Scientific, F530S) following the published protocol (*17*). Libraries were subjected to 151 bp paired-end sequencing according to the manufacturer's protocol on an Illumina NovaSeq 6000 at the University of Michigan Genomics core.

Bioinformatics

Sequencing reads were de-multiplexed using the Bcl2fastq2 Conversion Software (Illumina). Five prime end unique molecular identifiers (UMI, 9 nt random sequence) were used to remove PCR duplicates with a custom script. Then UMI and sequences and sequencing adapters were removed (fastx_clipper, 0.0.14). Reads were mapped to the Ensembl *D. melanogaster* genome (BDGP6) genome using Star (v 2.7.5a, (*27*)) with default settings (Table S4). Aligned reads were peak-called using Piranha (v 1.2.1) (*28*) (Data S1). Metagene analysis was performed using MetaPlotR (*29*). Crosslink induced mutation site analysis we performed as in (*17*). Sequence logo was generated using weblogo (v 2.8.2, (*30*)). Gene ontology (GO) analysis was performed using Gene Set Enrichment Analysis (GESA) implemented in the ClusterProfiler R package version 4.2.2 (*31*). We used Benjamini–Hochberg to correct for multiple hypothesis testing and "biological process" from the Bioconductor package "Genome Wide Annotations for Fly" version 3.8.2 for GESA (*32*).

Polysome fractionation

Polysome profiles were performed as previously described (*33*). Briefly, 300 fly heads were homogenized using a bead beater (Bead Ruptor, 19-040E) in 800 ul polysome extraction buffer (300 mM NaCl, 50 mM Tris-HCL (pH 7.5), 10 mM MgCl2, 200 mg heparin/ml, 400 U RNasin/ml, 1.0 mM, phenylmethylsulfonyl fluoride, 0.2 mg/ml cycloheximide, 1% Triton X-100, 0.1% sodium deoxycholate) then incubated on ice for 10 minutes. Lysate was cleared by centrifugation at 10,000 x g for 10 min at 4 °C. Equal A260 units were layered onto a 10–50% sucrose gradient in resolving buffer (20mM Tris-HCl (pH7.5), 150mM NaCl, 15mM MgCl2, 1mM DTT, 100ug/mL cycloheximide) and separated using a Beckman SW41Ti rotor (30,000 rpm for 3 hr at 4 °C). The absorbance (254 nm) was monitored and 750 ul fractions were collected using a Brandel pump

bioRxiv preprint doi: https://doi.org/10.1101/2022.09.20.508712; this version posted September 20, 2022. The copyright holder for this preprint (which was not certified by peer review) is the author/funder, who has granted bioRxiv a license to display the preprint in perpetuity. It is made available under aCC-BY-NC-ND 4.0 International license.

set to a flow rate of 1.5mL/min. Equal molar concentrations of *Saccharomyces cerevisiae* enolase-2 (*Eno2*) transcript was added to all fractions before RNA isolation. Nucleic acid was precipitated from each fraction then pellets were resuspended in water and phenol chloroform extracted following the manufacturer's protocol (Invitrogen, 15596026). The RNA was precipitated with isopropanol and GlycoBlue. RNA was resuspended in 10 ul water and equal volumes from each fraction were reverse transcribed following the manufacture recommendations (Invitrogen, 18080085). Fractions 5-12 were probed for *dilp2* and *Eno2* by qPCR (Table S1).

qPCR

Reverse transcription was performed using SuperScript III (Invitrogen, 18080085) with 1 ug of total RNA as input and primed with oligo(dT) (Invitrogen, 18418012) according to the manufacturer's protocol for transcript abundance analysis. Quantitative-PCR was performed following manufacturer's directions (Applied Biosystems, 4367659) for all experiments. Primers were added at a 2.5 µM concentration in 20 ul reactions. Reactions were run on the StepOnePlus Real-Time PCR System (Applied Biosystems), and quantifications were normalized relative to the reference gene ribosomal protein 49 (*Rp49*) for transcript abundance or spike-in, *Eno2*, for polysome fractionation (delta Ct method).

Fat and lean mass analysis

Colormetric measurements of triglycerides (Stanbio, SB-2100-430) and protein (Pierce, PI23225) were done as previously described (*34*), where 1 biological replicate n=2 male flies. Flies were collected 3-5 days post eclosion and homogenized with a Bead Ruptor. Standard curves were generated for each to normalize the concentration of samples. Samples were quantified using a Tecan Spark plate reader at 562 nm for protein or 500 nm for triglycerides.

Immunofluorescence

Immunofluorescence was done essentially as (*35*). Male flies 3-5 days post eclosion were sorted then aged for 2-5 days on standard food. Flies were then fasted in vials with a wetted Kimwipe for 16-18 hours before dissection. Brains were dissected in PBS, fixed (4% paraformaldehyde aqueous solution in 1X PBS), blocked (10% normal goat serum, 2% Triton X-100, 1X PBS), and then incubated overnight in primary antibody (rat anti-dilp2 (1:500) (*36*), rabbit anti-dilp3 (1:500) (*37*)). After washing (3% NaCl, 1% Triton X-100, 1X PBS), brains were

bioRxiv preprint doi: https://doi.org/10.1101/2022.09.20.508712; this version posted September 20, 2022. The copyright holder for this preprint (which was not certified by peer review) is the author/funder, who has granted bioRxiv a license to display the preprint in perpetuity. It is made available under aCC-BY-NC-ND 4.0 International license.

then incubated at room temp overnight in secondary antibody: either goat anti-rat Alexa Fluor 647 (Invitrogen, A-21247) or goat anti-rabbit Alexa Fluor 488 (Invitrogen, A-11008). Brains were mounted in FocusClear (CelExplorer, FC-101) on coverslips, and the cell bodies were imaged using an FV1200 Olympus confocal with a 20x objective. Median intensity of individual insulin-producing cells was quantified using Fiji (*38*).

in vitro transcription for direct-RNA sequencing

DNA insulin templates were synthesized by IDT based on transcripts FBtr0076329 (fly *Dilp2*), NM_001185083.2 (mouse Ins2), and two randomized sequences containing only one adenine (Supplemental Table 2). To generate the salmon Ins template, we PCR amplified (Thermo Scientific, F530S) DNA from cDNA and Sanger sequence-verified the product (XM_014198195.2). Each template DNA sequence was used for *in vitro* transcription (Invitrogen, AM1334). To generate the randomized DNA template “rand-A” the reaction mixture contained bases adenosine, uracil, cytosine, and guanosine while the randomized DNA template “rand-m6A” used N6-methyladenosine in the palace of adenosine. All the other *in vitro* transcription reactions used only the standard bases. The reactions were performed following the manufacturer's protocol overnight.

Direct-RNA sequencing

500 ng of poly(A) selected (Invitrogen) RNA from heads of flies or a total 500 ng of pooled *in vitro* transcribed RNA was used for library preparation following the manufacturer's protocol (Oxford Nanopore, SQK-RNA002, Version DRS_9080_v2_revB_22Nov2018). Briefly, the RT adapter was ligated to the RNA, reverse transcription was performed, and the RNA-cDNA hybrids were purified. Next, the second adapter was ligated to the RNA and again purified. The libraries were loaded onto the MinION flowcell (R9.4.1). The Oxford Nanopore sequencer was run for 24-36 hours. Data were base called using Oxford Nanopore’s Guppy (v 3.1.5) and aligned to the reference sequences using MiniMap2 -ax splice -uf -k14 (v 2.17) (*39*). Only reads that passed filtering and that mapped to the reference were considered for further analysis. Next, aligned reads from biological samples (modified) and matched *in vitro* transcribed RNAs (unmodified) were used as input to EpiNano (EpiNano-Error, v 1.2) to determine the positions of modifications (*21*). We plotted the data from the longest transcript (NM_001185083.2) for EpiNano mouse data. The Tombo suite of tools was used to visualize reads (*40*).

Circulating glucose assay

bioRxiv preprint doi: https://doi.org/10.1101/2022.09.20.508712; this version posted September 20, 2022. The copyright holder for this preprint (which was not certified by peer review) is the author/funder, who has granted bioRxiv a license to display the preprint in perpetuity. It is made available under aCC-BY-NC-ND 4.0 International license.

Hemolymph was collected from starved (12-16 hours) male flies from 40-50 flies per replicate by centrifugation. Circulating glucose levels were measured as previously described (*41*). Briefly, 0.5 ul of hemolymph was added to 100 ul of HexoKinase (HK) reagent (Sigma, GAHK20), incubated at room temperature for 15 min, then absorbance at 340 nm was measured on a Tecan Spark plate reader.

Generation of *dilp2* m^{6}A mutant flies

CRISPR constructs were synthesized and micro-injected into *w1118* flies by Rainbow Transgenic Flies (Camarillo, CA). The pScarless donor vector (dsRed marker) was introduced to remove the endogenous Dilp2 3'UTR and replace it with a mutant Dilp2 3'UTR that replaced 11 AC dinucleotides to TC (Supplement Fig. 4A). F1 progeny were screened for transformation with dsRed fluorescence. Positive transformants were Sanger sequenced (below) to verify the correct insertion.

Sanger Sequencing

Genomic DNA was extracted from two male flies from each fly line with positive dsRed expression by silica column purification (Invitrogen, K182002). The *dilp2* locus was PCR amplified (Thermo Scientific, F-530XL), PCR products were purified and normalized to 5ng/ul with 10 pmol/ul of the with appropriate primer added. Samples were submitted to Eurofins Genomics for sequencing and traces were analyzed with Benchling software.

Mouse islet isolations

Islet cells were collected from 4 fasted male mice from Vil-Cre backcrossed to C57 9x by the University of Michigan Islet Isolation core. The pooled tissue was added directly to Trizol (Invitrogen, 15596018) and stored at -80 °C.

Salmon pancreatic tissue isolation

The Atlantic salmon used was approximately 2 years old and post-smolt. The pancreatic tissue from one individual was isolated from the surrounding pyloric caeca. Upon removal, the tissue was immediately added to Trizol and stored at -80 °C.

Supplementary Figures

bioRxiv preprint doi: https://doi.org/10.1101/2022.09.20.508712; this version posted September 20, 2022. The copyright holder for this preprint (which was not certified by peer review) is the author/funder, who has granted bioRxiv a license to display the preprint in perpetuity. It is made available under aCC-BY-NC-ND 4.0 International license.

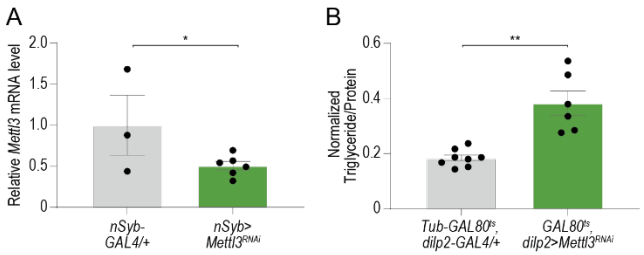

Supplementary Fig. 1. The effects of *Mettl3* KD on energy homeostasis are not developmental.

(A) Quantification of *Mettl3* mRNA from heads of control *Dilp2>w1118cs* and *Dilp2>Mettl3^{RNAi}* flies. n=3, 5 sets of 20 flies.

(C) Triglyceride levels normalized to protein in male control (*Tubulin-GAL80^{ts}, dilp2-GAL4* / +) and *Tubulin-GAL80^{ts}; dilp2>Mettl3^{RNAi}* flies. n=8, 6 pools of two flies. Error bars are SEM. Student's t-test. * $p < 0.05$

bioRxiv preprint doi: https://doi.org/10.1101/2022.09.20.508712; this version posted September 20, 2022. The copyright holder for this preprint (which was not certified by peer review) is the author/funder, who has granted bioRxiv a license to display the preprint in perpetuity. It is made available under aCC-BY-NC-ND 4.0 International license.

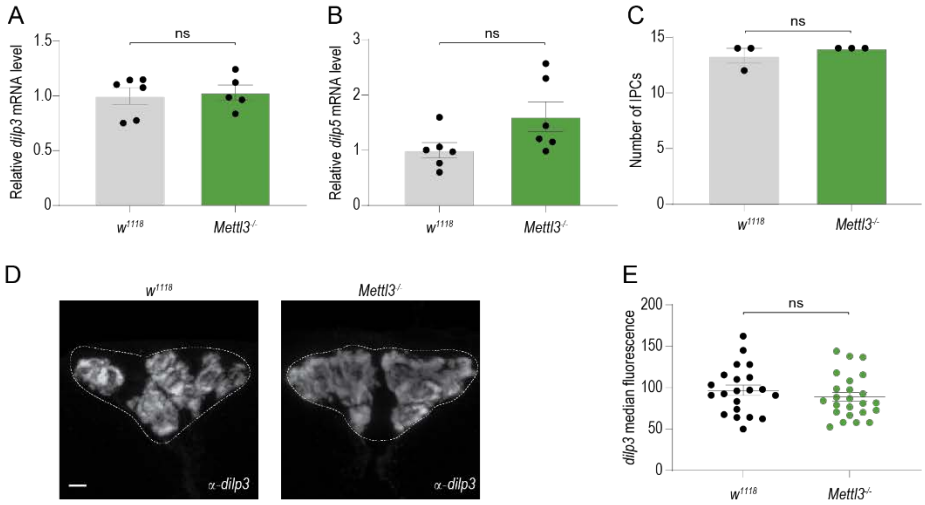

Supplementary Fig. 2. Additional phenotyping of *Mettl3* mutants.

(A, B) Quantification of (A) *dilp3* and (B) *dilp5* mRNA from heads of control ($w^{1118}CS$) and $Mettl3^{-/-}$ mutant flies. n=6 sets of 20 flies.

(C) Representative confocal images of immunofluorescence of *dilp3* protein in control ($w^{1118}CS$) and $Mettl3^{-/-}$ mutant flies. Scale bar, 20um.

(D) Quantification of median dilp3 fluorescence of individual insulin-producing cells from C), n=6 per genotype. Scale bar, 20um.

(E) Error bars are SEM. Student's t-test. ns = not significant, * $p < 0.05$.

bioRxiv preprint doi: https://doi.org/10.1101/2022.09.20.508712; this version posted September 20, 2022. The copyright holder for this preprint (which was not certified by peer review) is the author/funder, who has granted bioRxiv a license to display the preprint in perpetuity. It is made available under aCC-BY-NC-ND 4.0 International license.

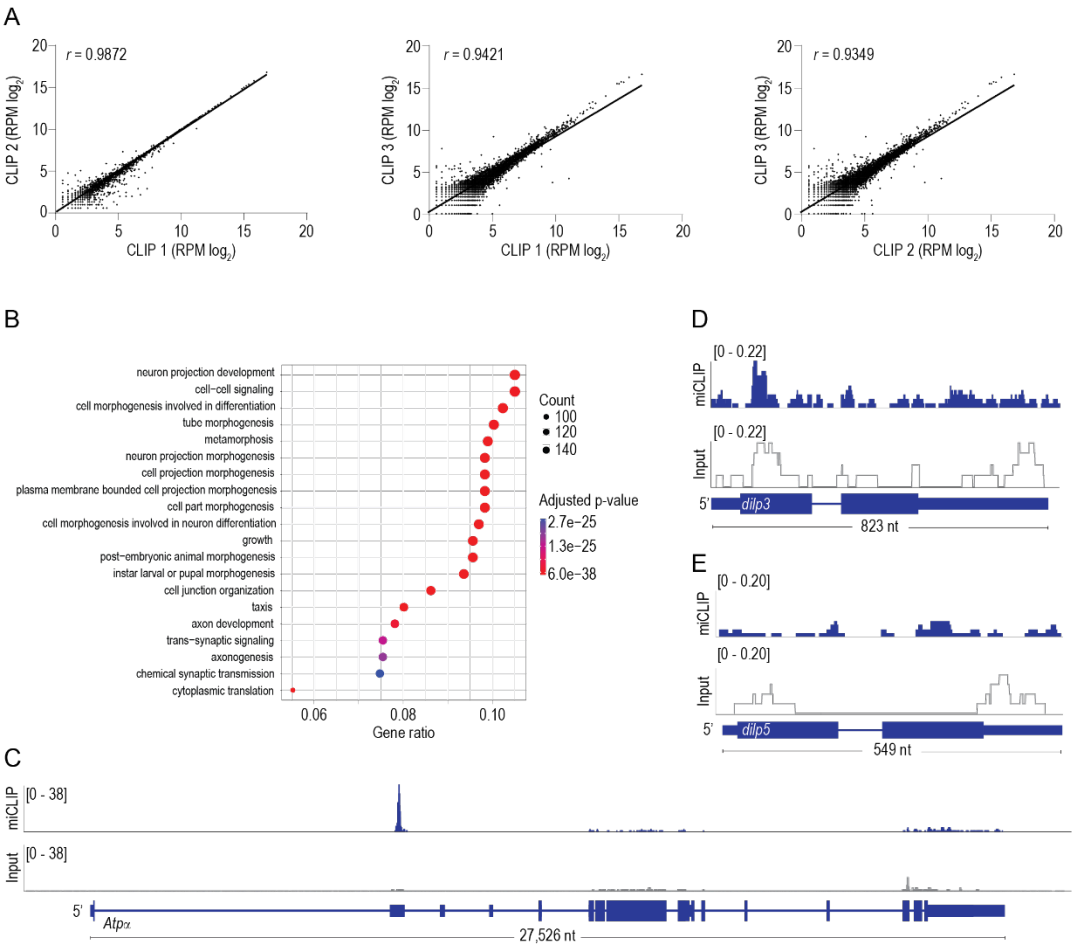

Supplementary Fig. 3. Reproducibility of biological CLIP replicates.

(A) Correlation plots of log2 normalized reads per CLIP peak. Each dot represents a CLIP peak found in all three biological replicates. Pearson's correlation coefficient (*r*).

(B) Gene ontology (GO) enrichment analysis of genes that harbor a CLIP peak. Circle size represents the number of genes that have CLIP peaks in the corresponding GO categories. The color represents the significance of the enrichment (Benjamini–Hochberg corrected p-value from Gene Set Enrichment Analysis (GSEA)).

(C, D, E) CLIP (blue) and input (gray) traces mapped to the *Atpα* (C), *dilp3* (D) and *dilp5* (E) loci (RPM).

bioRxiv preprint doi: https://doi.org/10.1101/2022.09.20.508712; this version posted September 20, 2022. The copyright holder for this preprint (which was not certified by peer review) is the author/funder, who has granted bioRxiv a license to display the preprint in perpetuity. It is made available under aCC-BY-NC-ND 4.0 International license.

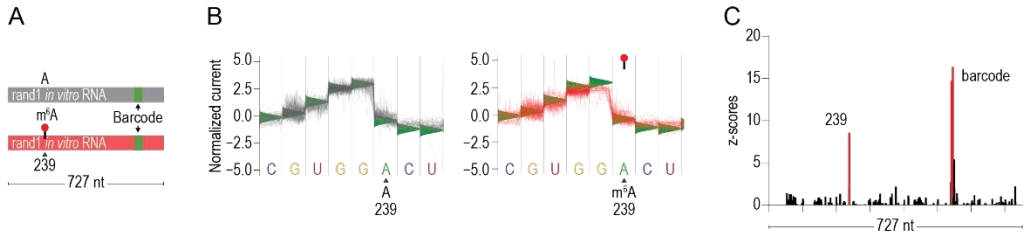

519

520 **Supplementary Fig. 4. Direct RNA sequencing of *in vitro* transcribed control RNAs.**

521

522 (A) Schematic of the randomly generated random-1 (rand1) *in vitro* transcribed RNAs. The
523 RNAs were transcribed with A (gray) and with m^{6}A (red). The sequences were identical except
524 for the 6 nt molecular barcode depicted by the green block to unambiguously distinguish
525 between the unmethylated and methylated RNA.
526 (B) Normalized direct RNA sequencing signal derived from direct RNA sequencing of *in vitro*
527 transcribed RNA with A (gray) and with m^{6}A (red). n=50 reads plotted. Green triangles represent
528 the expected current level based on the base calling mode used by Guppy (Version 3.1.5**,**
529 Oxford Nanopore Technologies).
530 (C) EpiNano significance trace across the *in vitro* transcribed RNA sequence. Significant
531 position 239 (red) corresponds to the base following the methylated A (238). Other significant
532 bases labeled “barcode” correspond to the green barcode in (A).

533

534

bioRxiv preprint doi: https://doi.org/10.1101/2022.09.20.508712; this version posted September 20, 2022. The copyright holder for this preprint (which was not certified by peer review) is the author/funder, who has granted bioRxiv a license to display the preprint in perpetuity. It is made available under aCC-BY-NC-ND 4.0 International license.

Wilinski et al.
Figure S5

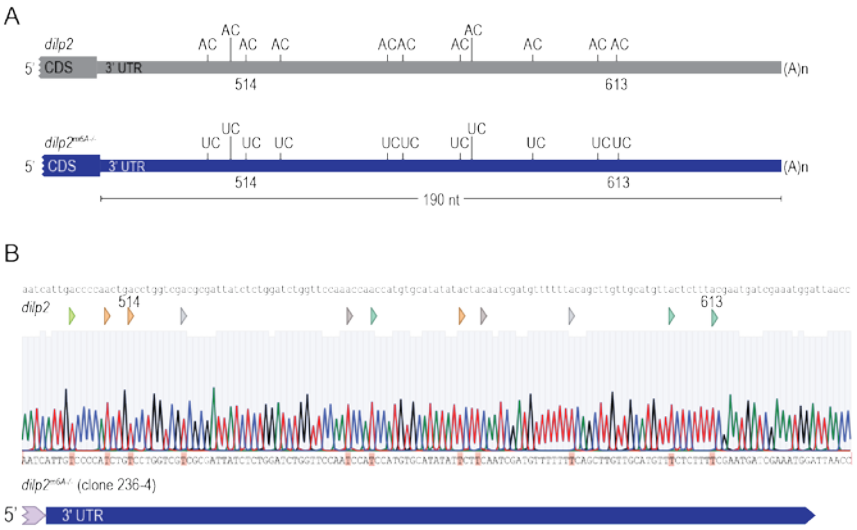

Supplementary Fig. 5. Creation of *dilp2*^{m6A} mutant flies.

(A) Diagram of CRISPR strategy to replace 11 AC dinucleotides in 3' UTR of the *dilp2* transcript (dilp2$^{m6A-/-}$gray).

(B) Sanger sequencing of genomic DNA from positive clone 364-4 showing all 11 AC dinucleotides replaced with UC.

bioRxiv preprint doi: https://doi.org/10.1101/2022.09.20.508712; this version posted September 20, 2022. The copyright holder for this preprint (which was not certified by peer review) is the author/funder, who has granted bioRxiv a license to display the preprint in perpetuity. It is made available under aCC-BY-NC-ND 4.0 International license.

Wilinski et al.
Figure S6

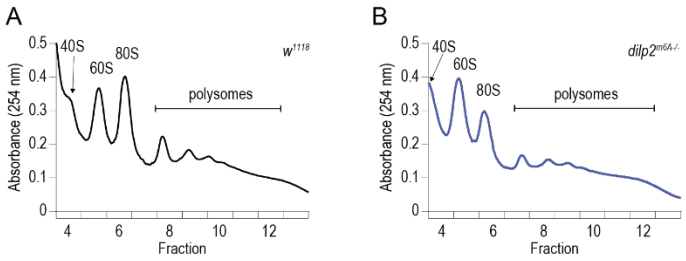

Supplementary Fig. 6. Polysome profiles of control and *dilp2*$^{m6A-/-}$ mutant flies.

(A, B) Representative polysome profile from sucrose gradient of (A) control (w^{1118}CS) and (B) *dilp2*$^{m6A-/-}$ mutant fly heads.

bioRxiv preprint doi: https://doi.org/10.1101/2022.09.20.508712; this version posted September 20, 2022. The copyright holder for this preprint (which was not certified by peer review) is the author/funder, who has granted bioRxiv a license to display the preprint in perpetuity. It is made available under aCC-BY-NC-ND 4.0 International license.

Primer name	**Sequence**
qPCR	
rp49	atcggttacggatcgaacaa
rp49	gacaatctccttgcgcttct
Ime4 qF	AAGGAACTCGTTGAGGCTGA
Ime4 qR	CACCTGTGTGGAGACAATGG
Dilp2-F	gaatcacgggattatactcctcg
Dilp2-R	atgagcaagcctttgtccttca
Dilp3-F	AGGATCCTGCTACCTAGCCTAC
Dilp3-R	ATTGAAGTTCACGGGGTCCAAAG
Dilp5-F	AGTTCTCCTGTTCCTGATCCCG
Dilp5-R	AATCGAATAGGCCCAAGGTGC
Sequencing *dilp2m6A* mutant	
Dilp2-F	aggagttcgaggaggaggataac
DsRed1-N	GTACTGGAACTGGGGGGACAG
DsRed1-C	AGCTGGACATCACCTCCCACAACG
Dilp2-R	ATCCTCCTCCTCGAACTCCTGG
CLIP	
CLIP 3' adapter	5rApp/tggaattctcgggtgccaaggaaaaaaaaaaaa/iAzideN/aaaaaaaaaaa/3Bio/
CLIP RT primer	/5Phos/gnnnnnnnngatcgtcggactgtagaactctgaac/IdSp/gccttggcacccgagaattcca
CLIP RNA PCR Primer (RP1)	AATGATACGGCGACCACCGAGATCTACACGTTCAGAGTTCTACAGTCCGA
CLIP RNA PCR Index Primers	CAAGCAGAAGACGGCATACGAGAT[6 bases]GTGACTGGAGTTCCTTGGCACCCGAGAATTCCA
***in vitro* transcribed RNA for direct-RNA sequencing**	
rand-1 barcode1	TAATACGACTCACTATAGGGAGAGGCCTTCCTCTGGGGGTTGTTGGTGCTCCTTTCCTTTTCGTTCGTTCGCGCGCGCGGGGTGTGTGTCTGCTGGTTTTCTCCTTGCGGTGGTGGCGCCTGGTGCCCTGGTTTCTCTTGCCGTCTCTGGGGTGTTTCTCGCCTTGCTTTGGCCGCTTGCGCTTGTCTCCTTGGTGTGTTTCTGTTGCGCTCCCTGGTGTCTCTTTCCGGTGGCCTGGACTGTGTGCGTC

bioRxiv preprint doi: https://doi.org/10.1101/2022.09.20.508712; this version posted September 20, 2022. The copyright holder for this preprint (which was not certified by peer review) is the author/funder, who has granted bioRxiv a license to display the preprint in perpetuity. It is made available under aCC-BY-NC-ND 4.0 International license.

	CCTTTTCGTGTCGGCGCGGTTGCTCCGTCCGCCCTTTGTTTGGCGCTCTT TTTCTTCCTCTTGTTTTTGGGTGCGCCTCTTTTGGCGGTCGGCCGGTCTT GCTCGGGCTTCCCTCGGTGCGCGGGCTTCGCGCCTTTTTGGGCTTGTGTC TCTTCGTCGTGTTCTTCGGGTCCCCTTGTTGTTTCGTCGGTCTTCTTGCC CTCGGGGCTTCGGTCTTTGCTCCTCCGTGCCTGTTGCCTTGTCCTTGTGG GCCCTCGTGTCCTTCGCGGCTGCGTTTGGGGCTTGTTGTGCTTTGTTCTC TTGTTCGTCCCTGTCTGTGTGCGTTGGCCCGCGGCTTTTGTTGTCTTTGC CTGCTGTCTCTTGGTCCGTGTTTTCTTTGCTTGCCGTTGTGCCGTCGGGT TGCCTTCGCGTGTTTCTGCGTCGTCTTTTTGGTTCCGTTTTTTTCCTCGC TCTTCCTGCGGCCTTTCTTCTTTGTTGTGTCCCTctgctctgttcgggcg
rand-1 barcode2	TAATACGACTCACTATAGGGAGAGGCCTTCCTCTGGGGGTTGTTGGTGCT CCTTTCCTTTTCGTTCGTTCGCGCGCGCGGGGTGTGTGTCTGCTGGTTTT CTCCTTGCGGTGGTGGCGCCTGGTGCCCTGGTTTCTCTTGCCGTCTCTGG GGTGTTTCTCGCCTTGCTTTGGCCGCTTGCGCTTGTCTCCTTGGTGTGTT TCTGTTGCGCTCCCTGGTGTCTCTTTCCGGTGGCCTGGACTGTGTGCGTC CCTTTTCGTGTCGGCGCGGTTGCTCCGTCCGCCCTTTGTTTGGCGCTCTT TTTCTTCCTCTTGTTTTTGGGTGCGCCTCTTTTGGCGGTCGGCCGGTCTT GCTCGGGCTTCCCTCGGTGCGCGGGCTTCGCGCCTTTTTGGGCTTGTGTC TCTTCGTCGTGTTCTTCGGGTCCCCTTGTTGTTTCGTCGGTCTTCTTGCC CTCGGGGCTTCGGTCTTTGCTCCTCCGTGCCTGTTGCCTTGTCCTTGTGG GCCCTCGTGTCCTTCGCGGCTGCGTTTGGGGCTTGTTGTcTgctcgtgTC TTGTTCGTCCCTGTCTGTGTGCGTTGGCCCGCGGCTTTTGTTGTCTTTGC CTGCTGTCTCTTGGTCCGTGTTTTCTTTGCTTGCCGTTGTGCCGTCGGGT TGCCTTCGCGTGTTTCTGCGTCGTCTTTTTGGTTCCGTTTTTTTCCTCGC TCTTCCTGCGGCCTTTCTTCTTTGTTGTGTCCCTctgctctgttcgggcg
in vitro RNA	TAATACGACTCACTATAGGGAGAGGCCTTCCTCTGGGGGTTGTTGGTGCTC CTTTCCTTTTCGTTCGTTCGCGCGCGCGGGGTGTGTGTCTGCTGGTTTTCT CCTTGCGGTGGTGGCGCCTGGTGCCCTGGTTTCTCTTGCCGTCTCTGGGGGT GTTTCTCGCCTTGCTTTGGCCGCTTGCGCTTGTCTCCTTGGTGTGTTTCTG TTGCGCTCCCTGGTGTCTCTTTCCGGTGGCCTGGACTGTGTGCGTCCCTTT TCGTGTCGGCGCGGTTGCTCCGTCCGCCCTTTGTTTGGCGCTCTTTTTCTT CCTCTTGTTTTTGGGTGCGCCTCTTTTGGCGGTCGGCCGGTCTTGCTCGGG CTTCCCTCGGTGCGCGGGCTTCGCGCCTTTTTGGGCTTGTGTCTCTTCGTC GTGTTCTTCGGGTCCCCTTGTTGTTTCGTCGGTCTTCTTGCCCTCGGGGCT TCGGTCTTTGCTCCTCCGTGCCTGTTGCCTTGTCCTTGTGGGCCCTCGTGT CCTTCGCGGCTGCGTTTGGGGCTTGTTGTGCTTTGTTCTCTTGTTCGTCCC TGTCTGTGTGCGTTGGCCCGCGGCTTTTGTTGTCTTTGCCTGCTGTCTCTT GGTCCGTGTTTTCTTTGCTTGCCGTTGTGCCGTCGGGTTGCCTTCGCGTGT TTCTGCGTCGTCTTTTTGGTTCCGTTTTTTTCCTCGCTCTTCCTGCGGCCT TTCTTCTTTGTTGTGTCCCTctgctctgttcgggcg
Ins2 gBlock	TAATACGACTCACTATAGGGAGAGGGGACCCAGTAACCACCAGCCCTAAGTGATC CGCTACAATCAAAAACCATCAGCAAGCAGGAAGGTTATTGTTTCAACATGGCCCT GTGGATGCGCTTCCTGCCCCTGCTGGCCCTGCTCTTCCTCTGGGAGTCCCACCCC ACCCAGGCTTTTGTCAAGCAGCACCTTTGTGGTTCCCACCTGGTGGAGGCTCTCT ACCTGGTGTGTGGGGAGCGTGGCTTCTTCTACACACCCATGTCCCGCCGTGAAGT GGAGGACCCACAAGTGGCACAACTGGAGCTGGGTGGAGGCCCGGGAGCAGGTGAC CTTCAGACCTTGGCACTGGAGGTGGCCCAGCAGAAGCGTGGCATTGTAGATCAGT GCTGCACCAGCATCTGCTCCCTCTACCAGCTGGAGAACTACTGCAACTAGACCCA CCACTACCCAGCCTACCCCTCTGCAATGAATAAAACCTTTGAATGAGCACAAAAA Aaaa
F Ins Ssalar-1	ACAAACATGCCTAACGAGGC

bioRxiv preprint doi: https://doi.org/10.1101/2022.09.20.508712; this version posted September 20, 2022. The copyright holder for this preprint (which was not certified by peer review) is the author/funder, who has granted bioRxiv a license to display the preprint in perpetuity. It is made available under aCC-BY-NC-ND 4.0 International license.

F Ins Ssalar-1 + T7	TAATACGACTCACTATAGGGAGAACAAACATGCCTAACGAGGC		
All primers are shown 5' to 3'			

552

553 **Table S1. Oligonucleotide sequences.**

554

555 DNA sequences used for qPCR primers, Sanger sequencing, CLIP adaptors, and in vitro

556 transcription of control RNAs.

557

bioRxiv preprint doi: https://doi.org/10.1101/2022.09.20.508712; this version posted September 20, 2022. The copyright holder for this preprint (which was not certified by peer review) is the author/funder, who has granted bioRxiv a license to display the preprint in perpetuity. It is made available under aCC-BY-NC-ND 4.0 International license.

	Lower case letter corresponds to position
***in vitro* transcribed randomized sequence-1**	
Position	sequence context
239	GGUGGCCUGGaCUGUGUGCGU
***Drosophila melanogaster* (fly)**	
Position	sequence context
519	AACUGACCUGgUCGACGCGAU
614	UUACUCUUUAcGAAUGAUCGA
644	CUUUGGCAAAcAAUCGC
***Salmo salar* (Atlantic salmon)**	
Position	sequence context
381	GCAGUGCUGUcACAAGCCCUG
464	CUCUCUGCCAcUCUCCAAUGC
495,496	CACCCCCGUCUaAAAGAUCUGC
549	UUUUAUUUUUcCUAGAAAAAU
***Mus musculus* (mouse)**	
Position	sequence context
34	UAAGUGAUCCgCUACAAUCAA
531	AACUAGACCCaCCACUACCCA
581	UGAAUGAGCAcAAAAAA

Table S2. Sequence context of significant direct-RNA sequence differences.

Sequences are listed for random *in vitro* transcribed RNA, and regions from native transcripts from each organism tested.

bioRxiv preprint doi: https://doi.org/10.1101/2022.09.20.508712; this version posted September 20, 2022. The copyright holder for this preprint (which was not certified by peer review) is the author/funder, who has granted bioRxiv a license to display the preprint in perpetuity. It is made available under aCC-BY-NC-ND 4.0 International license.

Fly line	Reference	Notes
Drosophila, w[1118]CS	A. Simon	CS and w1118cs from Seymour Benzer
Drosophila, w[1118]	Rainbow Transgenic Flies	
Drosophila, Ime4null (Mettl3)	Jean-Yves Roignant	backcrossed to w1118cs x 6
Drosophila, UAS-Ime4-HA/Cyo	Jean-Yves Roignant	
Drosophila, UAS-Mettl3RNAi: y[1] v[1]; P{y[+t7.7] v[+t1.8]=TRiP.GL01126}attP2/TM3, Sb[1]	Bloomington	41590
Drosophila, Dilp2-GAL4: w[*]; P{w[+mC]=Ilp2-GAL4.R}2/CyO	Bloomington	37516
Drosophila, nSyb-GAL4-2.1	Julie Simpson	
Drosophila, Tubulin-GAL80, dilp2-GAL4: w[*];Dilp2R-Gal4,TubP-Gal80[ts]/Cyo; +	Bloomington	
Drosophila *dilp2m6A*: w[1118];;Dilp2[m6A]/TM6C	This study	

Table S3. Fly stocks.

bioRxiv preprint doi: https://doi.org/10.1101/2022.09.20.508712; this version posted September 20, 2022. The copyright holder for this preprint (which was not certified by peer review) is the author/funder, who has granted bioRxiv a license to display the preprint in perpetuity. It is made available under aCC-BY-NC-ND 4.0 International license.

Table S4. Summary of sequencing reads.

Data S1. List of CLIP peaks.

Complete list of peaks from each biological replicate and the union of the data sets. CIMS output of C to T transitions.

bioRxiv preprint doi: https://doi.org/10.1101/2022.09.20.508712; this version posted September 20, 2022. The copyright holder for this preprint (which was not certified by peer review) is the author/funder, who has granted bioRxiv a license to display the preprint in perpetuity. It is made available under aCC-BY-NC-ND 4.0 International license.

Figure Legends

Wilinski et al.
Figure 1

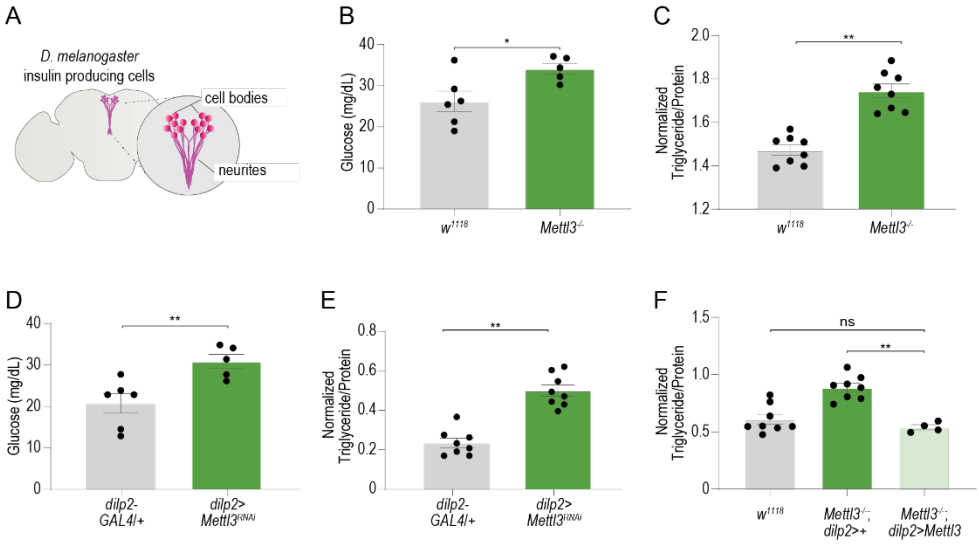

Fig. 1. Mettl3 is required for glucose balance and energy homeostasis in the insulin-producing cells.

(A) Diagram showing the location and anatomy of insulin-producing cells in the fly brain.
(B) The circulating hemolymph glycemia (n=6,) of fasted Mettl3$^{-/-}$ and *w1118* control flies.
(C) Triglyceride levels normalized to protein in male w^{1118}CS and mutant Mettl3$^{-/-}$ flies. n=8 pools of two flies.
(D) The hemolymph glycemia (n=6) of starved *dilp2>Mettl3^{RNAi}* and transgenic control flies.
(E, F) Triglyceride levels normalized to protein in male flies with cell-specific (E) knockdown (*dilp2>Mettl3^{RNAi}*) or rescue of (F) (*dilp2>Mettl3$^{-/-}$*) of Mettl3; n=4-8 pools of two flies. Student's t-test. Error bars represent standard error of the mean (SEM). *p<0.05, ** p<0.005.

bioRxiv preprint doi: https://doi.org/10.1101/2022.09.20.508712; this version posted September 20, 2022. The copyright holder for this preprint (which was not certified by peer review) is the author/funder, who has granted bioRxiv a license to display the preprint in perpetuity. It is made available under aCC-BY-NC-ND 4.0 International license.

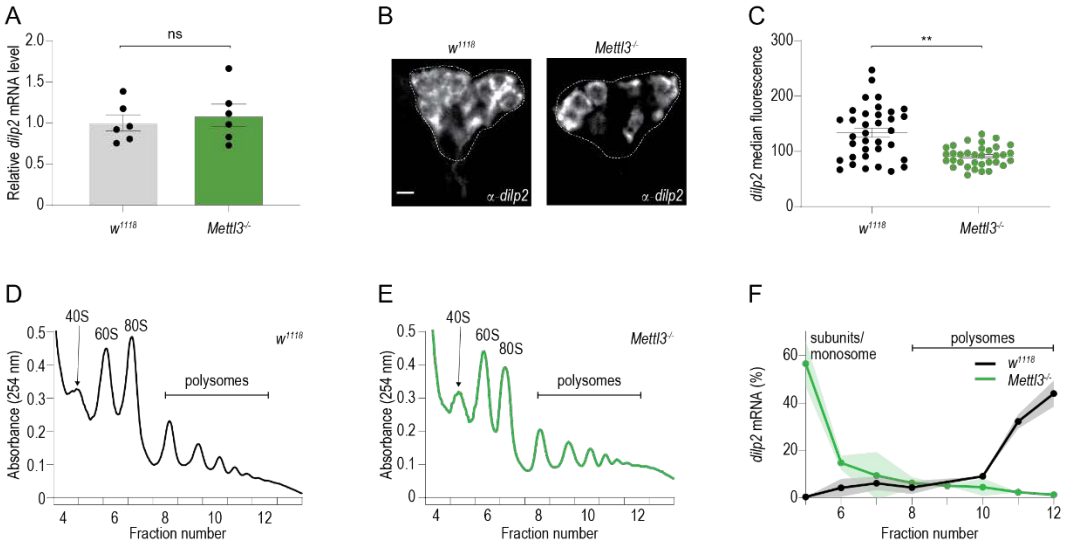

591

592 **Fig. 2. Mettl3 is required for the translation of *dilp2* mRNA**

593 (A) Quantification of *dilp2* mRNA from control and *Mettl3*$^{-/-}$ mutant flies. n=6 sets of 20 flies.
594 Error bars SEM in this and all subsequent panels. Student's t-test. ns =not significant
595 (p=0.5944).
596 (C) Representative confocal images of immunofluorescence of *dilp2* protein in control (w^{1118}CS)
597 and *Mettl3*$^{-/-}$ mutant flies. Scale bar, 20um.
598 (D) Quantification of median dilp2 fluorescence (arbitrary units) of individual insulin-producing
599 cells from *Mettl3* mutants and control flies; n=15 brains. Male flies were starved for 16 hr prior to
600 dissection and collected in 3 independent sets. Student's t-test. ** $p < 0.005$.
601 (E-F) Representative polysome profile from sucrose gradient of (E) control (w^{1118}CS) and (F)
602 *Mettl3*$^{-/-}$mutant fly heads (400).
603 (G) The proportion of *dilp2* mRNA in sucrose gradient fractions 5-12 normalized to spike-in RNA
604 from control (*w*^{1118}*CS*) and *Mettl3*$^{-/-}$ mutant flies. n=2, 400 heads per sample.

605

bioRxiv preprint doi: https://doi.org/10.1101/2022.09.20.508712; this version posted September 20, 2022. The copyright holder for this preprint (which was not certified by peer review) is the author/funder, who has granted bioRxiv a license to display the preprint in perpetuity. It is made available under aCC-BY-NC-ND 4.0 International license.

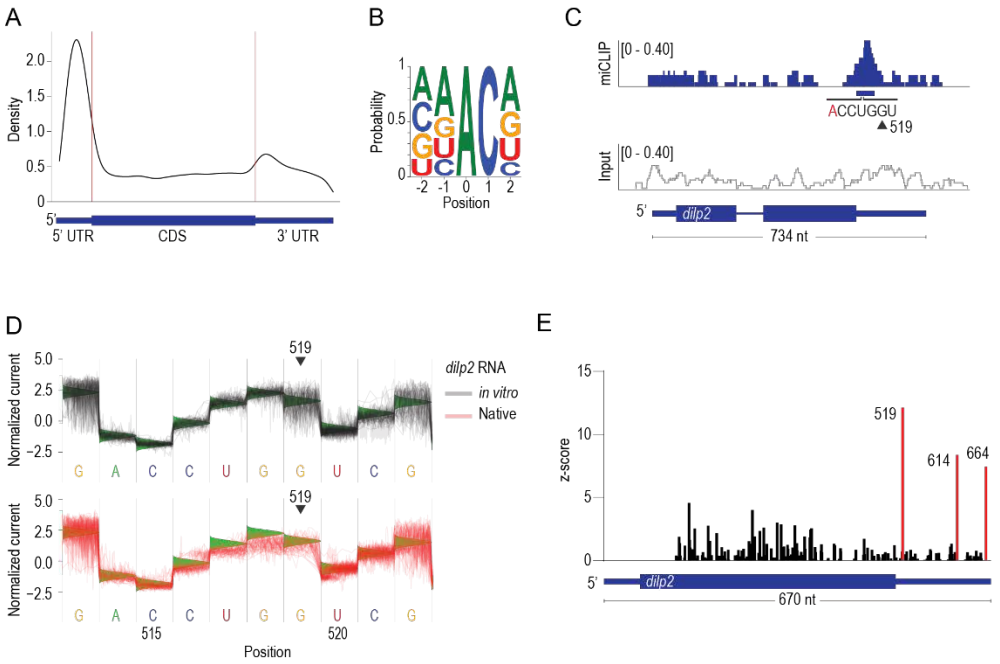

606

607 **Fig. 3. The 3' UTR of the *Drosophila melanogaster dilp2* mRNA is methylated.**

608 (A) Metagene plot of CLIP peaks from *D. melanogaster* head mRNA. Representing the position
609 of 4,506 CLIP peaks.
610 (B) The sequence context of 5,485 CIMS contained within CLIP peaks.
611 (C) CLIP (top, blue) and the no IP input control (bottom, grey) traces mapped to the dilp2 locus
612 (Reads Per Million mapped reads, RPM). The blue horizontal bar indicates the CLIP peak (FDR
613 <0.05) and the base composition flanking a putative m^6A site near position 519.
614 (D) Normalized direct-RNA sequencing signal derived from *in vitro* transcribed *dilp2* RNA (top,
615 gray, n=50 reads) and native *dilp2* mRNA from fly heads (bottom, red n = 50 reads) of the
616 region corresponding to the CLIP peak in (C). Green triangles represent the expected current
617 level based on the base calling model (see methods).
618 (E) EpiNano significance trace showing the nucleotide positions that are significantly different
619 (red bar, z-score > 6) between native and *in vitro* transcribed *dilp2* RNAs.

620

bioRxiv preprint doi: https://doi.org/10.1101/2022.09.20.508712; this version posted September 20, 2022. The copyright holder for this preprint (which was not certified by peer review) is the author/funder, who has granted bioRxiv a license to display the preprint in perpetuity. It is made available under aCC-BY-NC-ND 4.0 International license.

Wilinski et al.
Figure 4

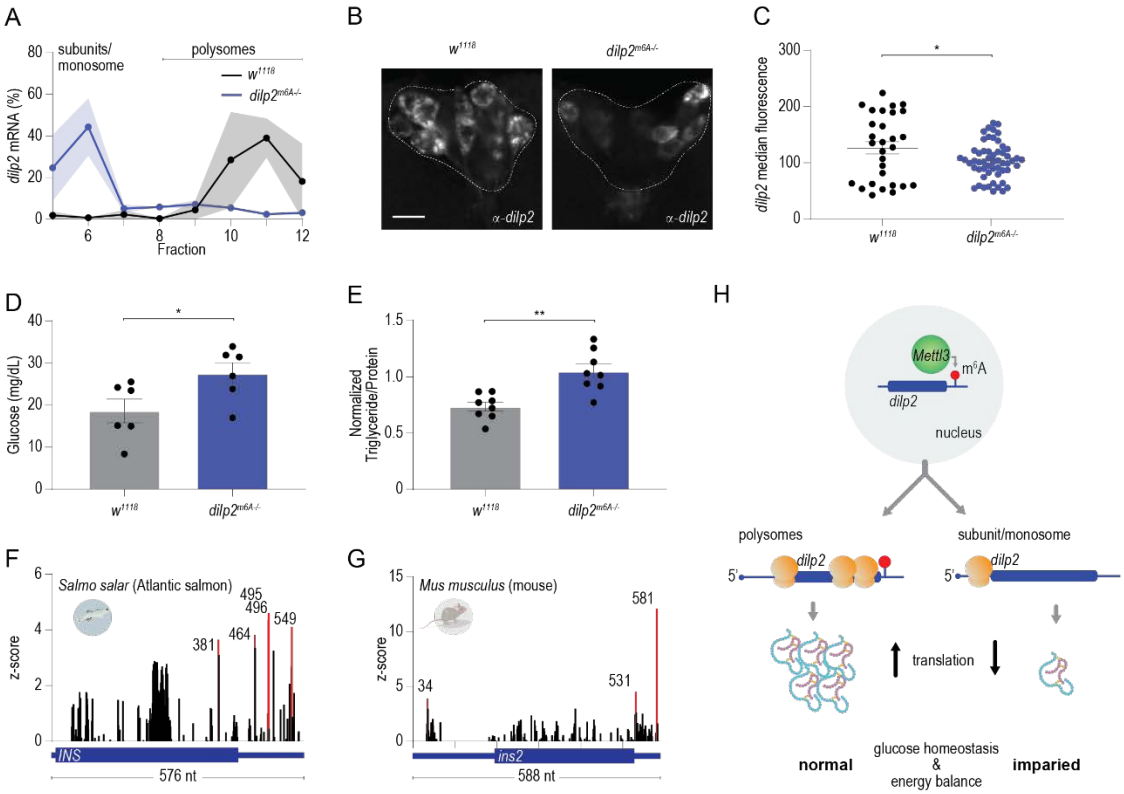

621

622 **Fig. 4. Methylation of dilp2 mRNA is necessary for robust translation.**

623 (A) Proportion of *dilp2* mRNA found in polysome gradient fractions 5-12 compared to a spike-in
624 RNA. n=3 samples of 400 heads each. Shading represents SEM.
625 (B) Representative confocal images of dilp2 protein in fasted control and *dilp2* $^{m6A-/-}$ mutant flies.
626 (C) Quantification of median *dilp2* fluorescence of individual insulin-producing cells from 6
627 brains from B). Scale bar, 20um. Error bars SEM. * $p<0.01$ Student's t-test.
628 (D) The circulating hemolymph glycemia (n=6) of fasted *dilp2* $^{m6A-/-}$ and control flies.
629 (E) Triglyceride levels normalized to protein in control (w^{1118}) and mutant *dilp2*$^{m6A-/-}$ flies. n=8
630 pools of two flies.
631 (F, G) Direct RNA sequencing significance trace comparing *in vitro* transcribed salmon INS (F)
632 or mouse INS2 (G) RNA to native mRNA isolated from salmon pancreatic tissue (F) or mouse
633 pancreatic islets (G). Numbers represent the significantly different nucleotides (red bar, z-scores
634 > 4 or >5) between native and *in vitro* transcribed RNAs.
635 (H) Model of translational control of *dilp2* RNA via m^6A. *$p < 0.05$, ** $p < 0.005$.